TU Delft

Delft University of Technology

Accuracy of noise prediction of propellers via numerical simulations, analytical methods, and experimental campaigns

Lima Pereira, L.T.; Ragni, D.; Romani, G.; Casalino, D.

DOI
10.2514/6.2024-3267

Publication date
2024

Document Version
Final published version

Published in
30th AIAA/CEAS Aeroacoustics Conference (2024)

Citation (APA)
Lima Pereira, L. T., Ragni, D., Romani, G., & Casalino, D. (2024). Accuracy of noise prediction of propellers via numerical simulations, analytical methods, and experimental campaigns. In *30th AIAA/CEAS Aeroacoustics Conference (2024)* Article AIAA 2024-3267 (30th AIAA/CEAS Aeroacoustics Conference, 2024). https://doi.org/10.2514/6.2024-3267

Important note
To cite this publication, please use the final published version (if applicable).
Please check the document version above.

Copyright
Other than for strictly personal use, it is not permitted to download, forward or distribute the text or part of it, without the consent of the author(s) and/or copyright holder(s), unless the work is under an open content license such as Creative Commons.

Takedown policy
Please contact us and provide details if you believe this document breaches copyrights.
We will remove access to the work immediately and investigate your claim.

This work is downloaded from Delft University of Technology.
For technical reasons the number of authors shown on this cover page is limited to a maximum of 10.

Aeroacoustics Conferences
June 4-7, 2024, Rome, Italy
30th AIAA/CEAS Aeroacoustics Conference (2024)

10.2514/6.2024-3267

Check for updates

Accuracy of noise prediction of propellers via numerical simulations, analytical methods, and experimental campaigns

Lourenço T. Lima Pereira*, Daniele Ragni†
Delft University of Technology, Delft, The Netherlands, 2628 CD

Gianluca Romani‡
Dassault Systemes Deutschland GmbH, Stuttgart, Germany, D-70563

Damiano Casalino§
Dassault Systemes Deutschland GmbH, Stuttgart, Germany, D-70563
Delft University of Technology, Delft, The Netherlands, 2628 CD

Downloaded by Technische Universiteit Delft on July 17, 2024 | http://arc.aiaa.org | DOI: 10.2514/6.2024-3267

This work focuses on the assessment of the accuracy of numerical prediction and experimental campaigns on providing the noise emissions of an isolated benchmark propeller. An experimental campaign is carried out with a model low-Reynolds propeller of 0.3 m diameter operating at high RPM, equivalent of a tip-Mach number (M_t) of 0.37 and an advance ratio (J) of 0.4. Measurements are conducted on an open-test section wind tunnel, surrounded by an anechoic chamber. Simulations are carried out with the commercial software PowerFLOW and aim at reproducing the propeller geometry and conditions. BEMT-based noise estimations are also used to demonstrate the expected results. The discussion is focused on the uncertainties of the experimental campaign, and the current accuracy of numerical and analytical predictions, creating a complete picture of the discrepancies expected when predicting propeller noise levels and potential sources of errors. Results point to an accurate ability of the three methodologies to assess the overall noise emissions. Nevertheless, precise description and measurements of the higher harmonics of the tonal emissions and of the broadband noise levels is still lacking and require improvements in experimental conditions and a detailed assessment of the flow over the propeller.

I. Nomenclature

x, y, z	=	Coordinate system with respect to propeller centre
BPF	=	Blade Passing Frequency
D	=	Propeller diameter
f	=	frequency [Hz]
J	=	Advance ratio
M_t	=	Propeller tip Mach number
n	=	Propeller rotational speed in rotations per minute [RPM]
N	=	Propeller number of blades
p'	=	Pressure fluctuations [Pa]
PSD	=	Power Spectral Density [dB, reference of 4×10^{-10} Pa^2/Hz]
Re_t	=	Propeller tip Reynolds number
SPL	=	Sound Pressure Level [dB, reference of 4×10^{-10} Pa^2]
U_∞	=	free stream velocity
ϕ	=	Azimuthal angle with respect to propeller plane of rotation

*Assistant Professor, Delft University of Technology, L.T.LimaPereira@tudelft.nl, and AIAA Member.
†Associate professor, Delft University of Technology, and AIAA Member.
‡Software Engineering Manager, Fluid Science & Technology, SIMULIA R&D.
§Full Professor, Delft University of Technology, Application Manager & Software Engineering Director, Fluid Science & Technology, SIMULIA R&D.

Copyright © 2024 by Lourenco Tercio Lima Pereira, Daniele Ragni, Gianluca Romani, Damiano Casalino.
Published by the American Institute of Aeronautics and Astronautics, Inc., with permission.

Downloaded by Technische Universiteit Delft on July 17, 2024 | http://arc.aiaa.org | DOI: 10.2514/6.2024-3267

II. Introduction

The application of aerial vehicles in urban environments is seen as a potentially viable commercial solution for last-mile transport of parcels and even transport of passengers [1]. Aerial vehicles designed for both applications have in common the exploration of electric motors and rotors, most of them consisting of a combination of open propellers. The latter often brings advantages of propulsive efficiency, enabling the use of electric motors and heavy batteries. However, propellers are also responsible for significant noise emissions, which is considered one of the key factors that will enable or block the application of aerial vehicles in urban environments [2].

Therefore, the prediction of noise and design of efficient and silent propellers has been the focus of attention of many designs and academic studies [3–5]. The spectrum of noise emitted by propellers is composed of two components, i.e. a tonal and a broadband one [6]. In most conditions, the former dominates the overall emissions from an isolated propeller. However, for small drones and urban air mobility vehicles, this figure can be different. The low-Reynolds number of operations of propellers for small drones and the potential turbulent flow field in which they fly cause the relevance of broadband components to rise. Besides, the low rotational speeds of the large propellers for urban air mobility shift the formerly dominant first tonal components to very low frequencies, in which human perception is very low. In this scenario, the relevance of the highest harmonics of the noise is fundamental.

These figures suggest a condition in which an accurate prediction, modelling, and experimentation of tonal, in all of its harmonics, and broadband noise from propellers are fundamental for the correct interpretation of noise emissions from novel urban air transportation systems. On that aspect, several works have been dedicated to the assessment of noise from clean propellers. Casalino et al. (2021) [7] have first proposed a benchmark propeller geometry and accompanying experiments describing the flow and acoustic properties of the propeller. Their results have been later used for the assessment of numerical simulations, yielding good agreement with broadband and tonal components [8]. Casalino et al. (2023) [5] have shown that a better match of flow field and noise emissions is obtained when the recirculation in the room is also considered. Nevertheless, discrepancies still exist and are mostly attributed to experimental uncertainties, motor and background noise, and simplifications of the numerical model.

This research is dedicated to a discussion on the currently achievable accuracy of experimental, numerical, and analytical techniques for evaluating the noise of an isolated propeller. A dedicated experimental campaign carried out followed equivalent analytical prediction and numerical simulations. The levels of the tonal and broadband noise accuracy captured from the methodologies are used to create an oriented discussion in the difficulties encountered on the noise predictions from isolated propellers and the sources of possible discrepancies between the different methodologies.

III. Experimental Campaign

A. Model, facility, and conditions

Experiments are conducted in the A-Tunnel facility of Delft University of Technology [9]. The open-test section wind tunnel encompasses an anechoic room of $6.4 \times 6.4 \times 3.4$ (height) m^3 designed to absorb acoustic waves above 150 Hz. The flow enters the test section through a cylindrical nozzle of 0.6 m diameter. Flow speeds of up to 34 m/s can be achieved with turbulence intensities below 0.01%.

A benchmark propeller model is used for the tests. The model propeller is based on an APC 9×6 propeller scaled to 0.3 m diameter, using NACA 4412 airfoil geometry. The propeller geometry is described in the work of Grande et al. [10]. The propeller is mounted 0.3 m from the nozzle exit on a propeller rig. The propeller is driven by a Leopard Hobby 3536-5T 1520 KV motor. The motor is attached to a 6-axes load cell by Futek. A Digital EM1 differential optical encoder is used to control the propeller RPM and reference the propeller position during the acoustic acquisition.

Measurements are carried out with the propeller at 8,000 rotations per minute (RPM) and with 16 m/s flow speed, corresponding to an advance ratio of 0.4 and tip Mach number of 0.37, as summarized in Table 1. The choice of conditions is deemed more representative of real applications when compared to previous validations carried at smaller tip Mach numbers [4]. Besides, the high-pitch propeller geometry selected yields non-ideal flow conditions at low advance ratios, with more controlled conditions reflected at the selected advance ratio.

B. Acoustic measurements

Acoustic measurements are carried out with a microphone arc consisting of 7 microphones. The microphones are placed at 1 meter from the propeller centre of rotation and describe azimuthal angles from -20 to 60° with 10° step. Figure 1 shows the microphone arc, the propeller setup, and the geometric description of the experiment.

Table 1 Conditions of the tested propeller.

Parameter	Symbol	Value
Propeller diameter (m)	D	0.30
Propeller number of blades	N	2
Propeller rotational speed (RPM)	n	8,000
Flow speed (m/s)	U_∞	16.0
Advance ratio	$J = \frac{60U_\infty}{D.n}$	0.40
Tip Mach number	M_t	0.37
Tip Reynolds number	Re_t	89,000
Blade Passing Frequency (Hz)	BPF	267

Acquisition is controlled by a PXI express system with microphones connected to PXIe-4499 boards with 24 bits precision. Acoustic acquisitions are carried out for 30 seconds with a sampling rate of 102,400 samples per second. The microphones used are GRAS 46BE with flat response from 10 to 40 kHz (1 dB precision). Calibration of the microphones is carried out in situ using a GRAS 42AG pistonphone operating at 1,000 Hz (94 dB sound pressure).

IV. Numerical Simulation

Simulations are carried out using a setup similar to previous works that numerically assessed noise from the same propeller[4]. In the setup, only the geometries of the propeller and the motor nacelle are considered.

Numerical simulations are based on the commercial software SIMULIA PowerFLOW. The software uses the Lattice-Boltzman Method (LBM) applied to a cartesian mesh. A two-equation $\kappa - \epsilon$ turbulence model is selected for the gas relaxation properties. Noise emissions at the microphone locations are obtained by a standard time-domain FW-H, Formulation 1A described in Farassat [11], in forward time [12]. The simulation is carried out for 50 revolutions to ensure precise description of low-frequency tonal components. The reader interested in more details on the simulation conditions is referred to the work of Casalino et al.[7].

V. Blade Element Momentum Theory (BEMT) based noise estimation

For comparisons with expected results from the theory of propeller noise, BEMT-based noise estimation is also carried out. The BEMT-based noise estimations follow the works of [7, 13]. The flow model follows conventional BEMT formulation for uniform inflow and includes Prandtl tip-losses. Lift and drag coefficients from the airfoil sections are obtained from a potential flow solver coupled with a boundary layer model, following [14].

From the aerodynamic force distribution, the tonal sources are estimated based on a time-domain description of moving compact distributed dipole sources for the load noise and monopole ones for the thickness noise [13]. Broadband noise estimations follow the work of Roger & Moreau [15] adapted for a rotating framework [16]. The turbulent boundary layer wall-pressure spectra required for the estimations are obtained from Schlinker's model [16].

VI. Results and Discussions

A. Experimental results

The spectrum of the propeller noise is shown in Figure 2 for the entire frequency range (a) and the details of the first 10 BPFs (b). The spectrum also shows the measured noise of the isolated motor operating at the same RPM. It is worth mentioning that the different torque demanded from the motor in the two conditions alters the noise emitted by the motor. Nevertheless, it can be observed that the motor noise is responsible for affecting significantly the 3rd, 6th and 7th BPF of the measured spectrum. The latter BPF harmonic is related to the number of poles from the motor used (14). The first two are, most probably, due to the 3 phase operation of brushless motors. Some sub-harmonic tones are also observed. Those can be caused by asymmetries on the propeller geometry or again by the noise of the isolated motor. By comparing the isolated motor component against the propeller measurement, one can observe that the sub-harmonics are mostly present in the propeller one. This points to the first hypothesis, i.e. asymmetries from the

Downloaded by Technische Universiteit Delft on July 17, 2024 | http://arc.aiaa.org | DOI: 10.2514/6.2024-3267

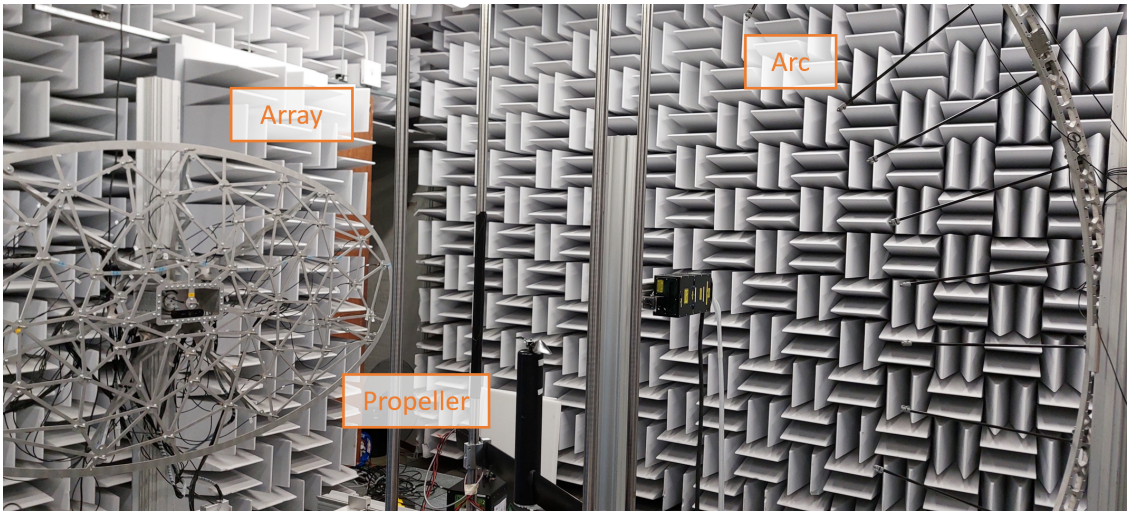

(a)

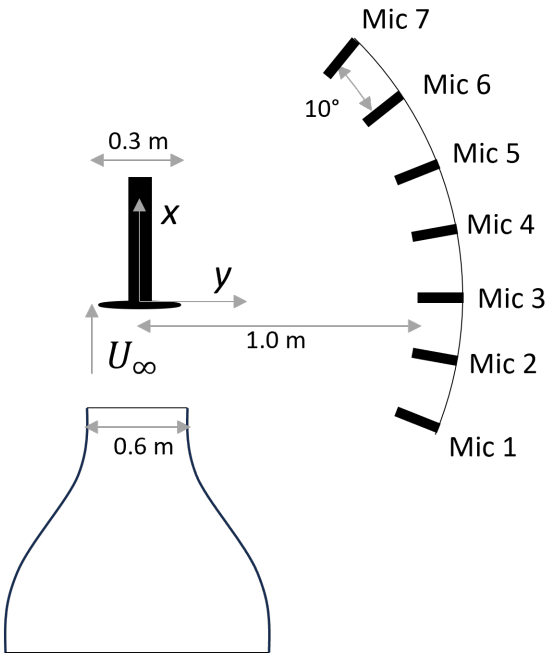

(b)

Fig. 1 Experimental setup and geometry.

propeller or propeller mounting cause the sub-harmonic sources.

To better describe the tonal component of the noise from the propeller, Figure 3 shows the time history of pressure along one full rotation of the blade. The pressure fluctuations are obtained by the average of the pressure signal along the blade rotation, obtained from the signal of the encoders. The maximum deviations from the average time history are shown in shades of blue, encompassing the contribution from broadband noise components and deviations from the average tonal time history. By this process, the tonal component of the noise is removed from the broadband one. The root-mean-square of the pressure fluctuations yields a tonal noise emission of 84.4 dB. Similarly, the pressure fluctuation of the isolated motor is also provided, which totals 67.4 dB. The latter is seen at a higher frequency, following the observations from the spectrum.

Downloaded by Technische Universiteit Delft on July 17, 2024 | http://arc.aiaa.org | DOI: 10.2514/6.2024-3267

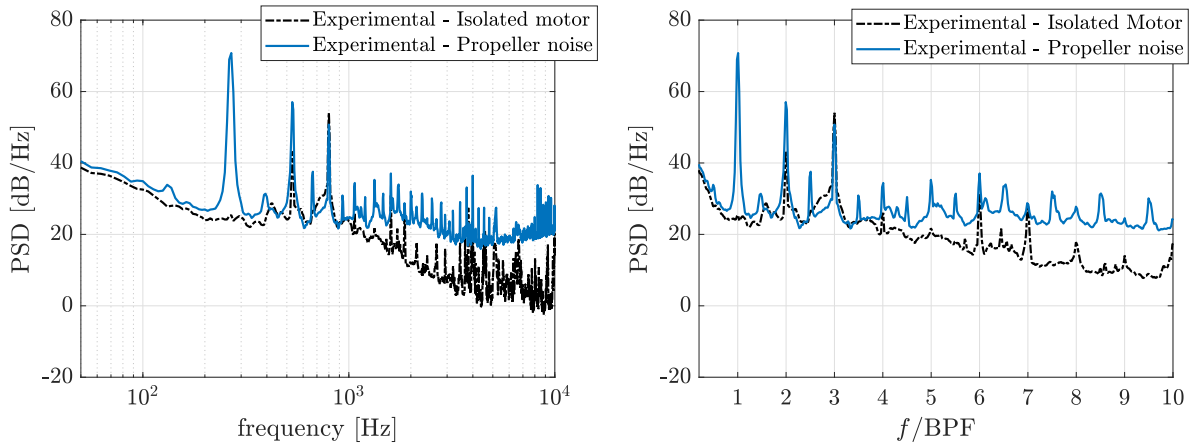

(a) Logarithmic (b) Linear

Fig. 2 Experimental acoustic spectrum of the propeller at $\phi = 0^o$ compared to the one of the isolated motor (a). (b) details the first tonal components of the spectrum.

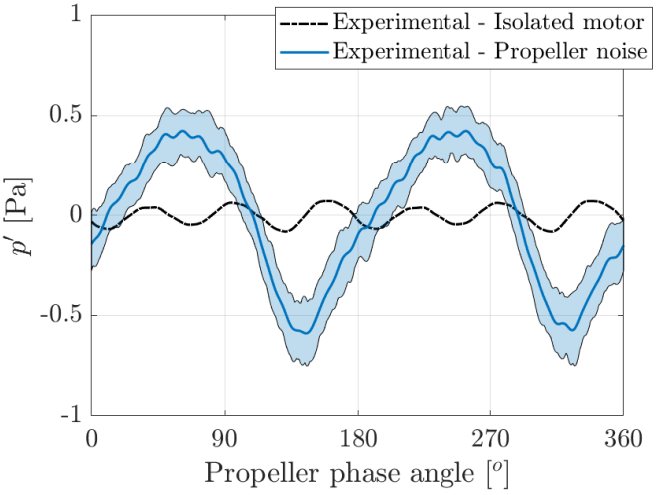

Fig. 3 Experimental average time history of the acoustic pressure fluctuations of the propeller at $\phi = 0^o$ compared to the one of the isolated motor. Blue shades show maximum and minimum level deviation with respect to the pressure time-history acquired.

1. Experimental uncertainties

Experimental techniques are prone to uncertainties and accurate measurements of tonal noise are particularly challenging. To start, the microphones used deliver a flat frequency response, single sensitivity in all frequency range, with $\epsilon_{\text{mic.}} = \pm 1$ dB. This is the maximum accuracy achievable with the current setup.

Besides the measuring equipment, controlling the RPM of the motor can be a cause of deviations. Figure 4 shows the histogram of RPMs captured during the data acquisition process. Overall, the RPM is controlled at an average of 7,998 RPMs with a maximum dispersion of ±20 RPMs. By considering that tonal noise scales with the RPM according to a 6^{th} power law, the error associated with the RPM variation is lower than $\epsilon_{\text{RPM}} = \pm 0.1$ dB.

Asymmetries in the flow or of the propeller geometry are another relevant source of uncertainties. The presence of non-uniform, unsteady force distribution over the blades significantly modifies the emissions from a propeller. The works of Goyal et al. and Monteiro et al. [17, 18] have demonstrated how small modifications of the loading along a rotation can have a significant impact on the emitted noise. Within the average time-history of pressure fluctuations, the

Downloaded by Technische Universiteit Delft on July 17, 2024 | http://arc.aiaa.org | DOI: 10.2514/6.2024-3267

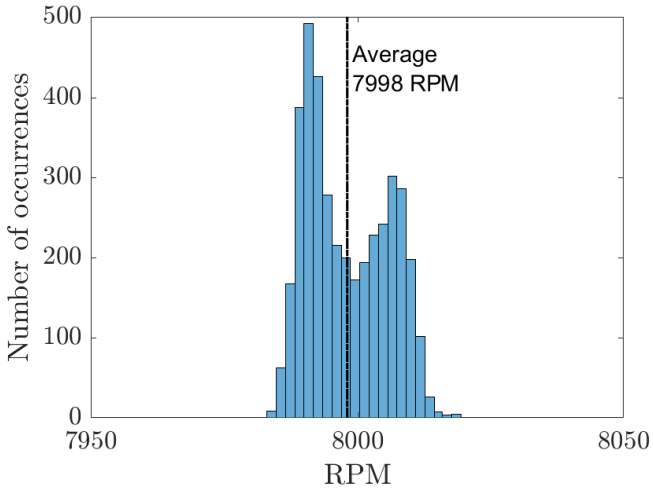

Fig. 4 Experimental histogram of the RPM measured along the acoustic acquisition.

effect of asymmetry between the propellers can be inferred by the deviation of the time-history during each half of a rotation. Given the symmetry of the problem, the generated spectrum from the time history of the first half of rotation should be exactly the one of the second half. Deviations from that would indicate problems with the symmetry assumed on both blades In the current experiment, the standard deviation of the time history between the first and second blade passing is 0.022 Pa, resulting in a possible change of the tonal noise levels of $\epsilon_{\text{geo.}} \pm 0.6$ dB (one standard deviation).

A final source of uncertainty is given by acoustic reflections along the chamber. The structures required for the setup, i.e. acoustic arc structure, propeller rig, nozzle, and accessories disturb the reflective properties of the anechoic chamber and, importantly, deviate from the simulated conditions. Reflections are responsible for possible constructive and destructive interference that can modify the measured levels. This source of error is hard to take into account as it can cause total cancellation or doubling of the source and, in this work, it is mitigated by increasing the spatial distribution of sensors and comparing results for all the azimuth angles measured.

In summary, it is extremely challenging to predict the uncertainty of microphone measurements, especially if reflections are to be considered. By neglecting the letter and applying error propagation theory, a deviation of ±1.7 dB is expected for the current experiment conducted.

B. Comparisons of tonal noise

A first comparison between tonal predictions and experimental results shows the spectrum of the sound pressure level (SPL) captured with both techniques at different azimuthal angles (Figure 5). The results are presented in SPL for the accurate comparison of the tonal components. Nevertheless, the experimental, numerical, and analytical spectra are obtained with a frequency discretization of 25, 22.6, and 15 Hz respectively, and comparisons of the broadband signal are also fairly possible (0.4 dB lower for the numerical case and 2.2 dB higher for the analytical model).

As observed, the numerical simulation and analytical model represent fairly well the level of the first BPF of the propeller noise in comparison to the experiments, with the measured tone being 0.2 dB higher than the predicted one from the BEMT and 0.3 dB from the numerical one. The second harmonic, however, shows larger discrepancies, with the measurements demonstrating a tone 2.7 dB higher than the BEMT predictions and 1.5 dB higher than the numerical ones. The higher harmonics demonstrate much higher uncertainties. To these, the precision of the experiments hampers the comparisons. The third harmonic, as mentioned before is affected by the electric noise and experimental values cannot be compared. Amongst BEMT and numerical data, discrepancies are in the order of 0.7 dB for the azimuthal angle $\phi = 0^o$.

The averaged time history of pressure along one full rotation of the blade is again shown in the comparison between the BEMT-based predictions, experimental, and numerical results in (Figure 6). The maximum deviations from the average time history are shown in shades of blue for the experiments and of red for the numerical simulations. As observed, the agreement between the average pressure time histories follows the predictions of the first and second BPFs. Discrepancies are observed on the higher negative pressure peak from the experimental time history and the

Downloaded by Technische Universiteit Delft on July 17, 2024 | http://arc.aiaa.org | DOI: 10.2514/6.2024-3267

Downloaded by Technische Universiteit Delft on July 17, 2024 | http://arc.aiaa.org | DOI: 10.2514/6.2024-3267

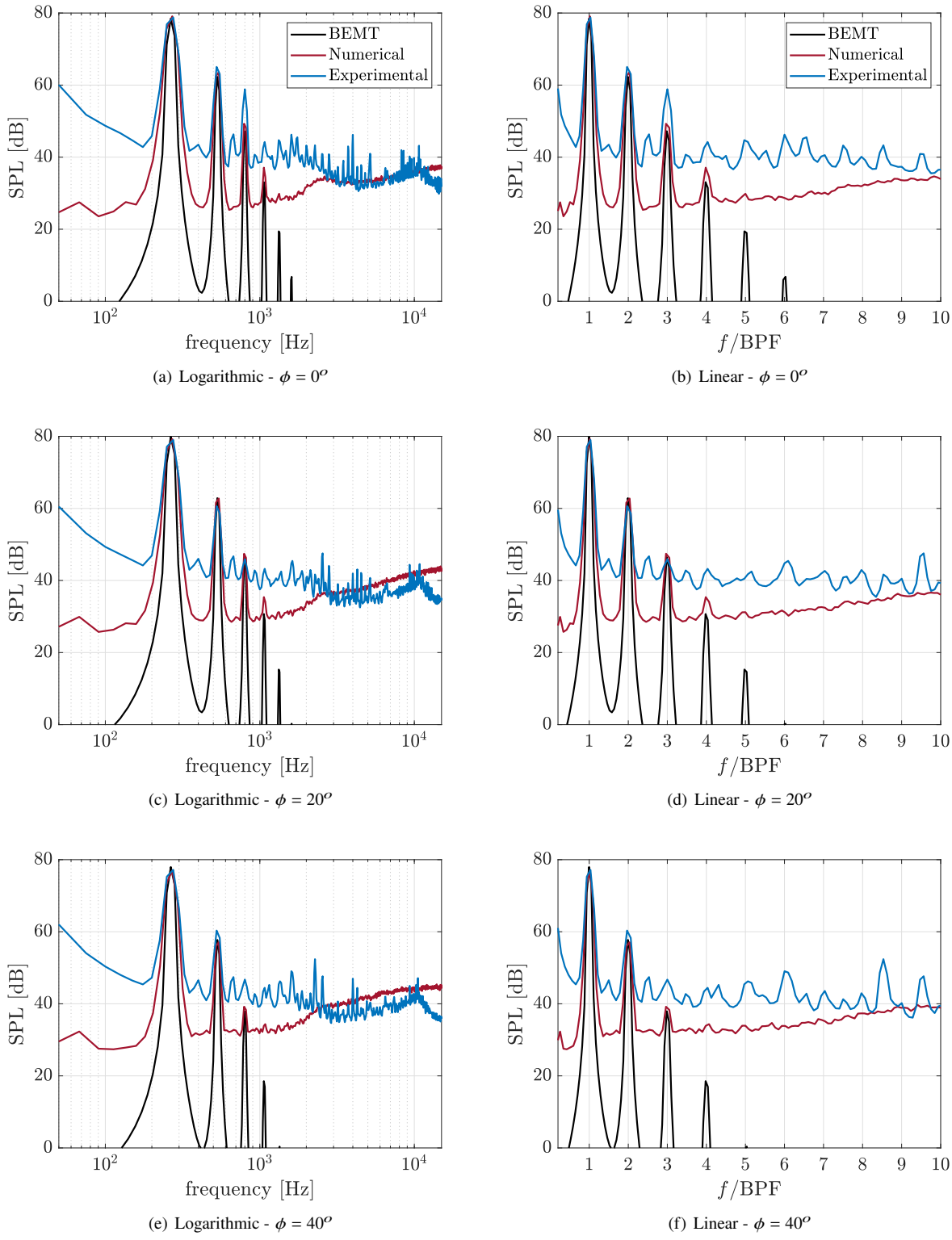

(a) Logarithmic - $\phi = 0^o$

(b) Linear - $\phi = 0^o$

(c) Logarithmic - $\phi = 20^o$

(d) Linear - $\phi = 20^o$

(e) Logarithmic - $\phi = 40^o$

(f) Linear - $\phi = 40^o$

Fig. 5 Experimental, numerical, and BEMT-based acoustic spectrum of the propeller at $\phi = 0^o$ compared to the one of the isolated motor (a). (b) details the first tonal components of the spectrum.

lower estimated one from the analytical method. Both are more evident for $\phi = 0^o$.

Between numerical simulations and experimental measurements, the level of the broadband fluctuations is well captured and the mean pressure signal is well in agreement. Nevertheless, deviations exist. In particular, the broadband signal numerically predicted from the blades is higher when the average pressure has a negative derivative, i.e. pressure fluctuations are decreasing. This phenomenon indicates a modulation of the broadband signal, attributed to the dominance of trailing-edge noise, and its varying directivity as the propeller rotates [19]. The latter reference has observed, experimentally, the modulation effect over the same propeller at different conditions. In this study, the modulation is observed in the experimental data mildly. Reasons for that are the presence of stronger low-frequency broadband components, possibly related to turbulence impingement noise and background noise from the wind tunnel.

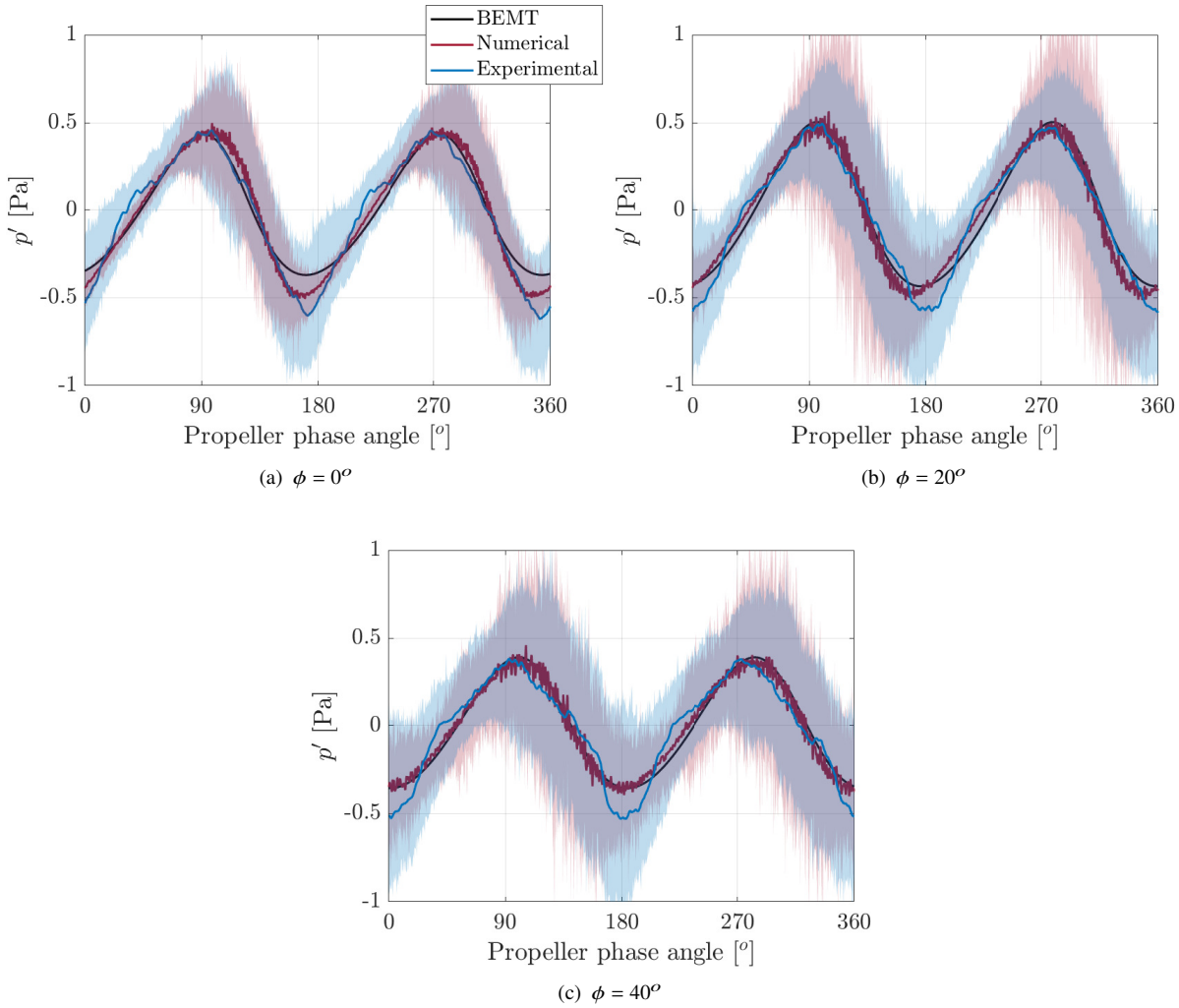

(a) $\phi = 0^o$ (b) $\phi = 20^o$

(c) $\phi = 40^o$

Fig. 6 Experimental, numerical, and BEMT-based average time history of the acoustic pressure fluctuations of the propeller at $\phi = 0^o$. Blue and red shades show maximum and minimum level deviation with respect to the pressure time-history captured experimentally and numerically respectively.

The directivity of the tonal sources, obtained from the bandpassing of the average time signal, is shown in Figure 7 for the 6 first harmonics of the BPF. The methodology is used to filter broadband signals from the tonal components, allowing comparisons of the latter for higher harmonics, where the broadband levels dominate. Predictions of the first two BPFs demonstrate agreement between the three methodologies, with larger discrepancies shown for the BEMT-based methodology. Directivity patterns agree well with each other with slightly lower levels from the analytical method towards upstream. Stronger differences are observed for the higher harmonics. Experimental results struggle with motor noise that affects the 3rd and 6th BPFs. Still, higher BPF harmonics demonstrate agreement between BEMT-based

Downloaded by Technische Universiteit Delft on July 17, 2024 | http://arc.aiaa.org | DOI: 10.2514/6.2024-3267

predictions and experiments, while numerical methods seem to significantly underpredict noise levels. In general, numerical methods and analytical ones agree fairly well in directivity patterns up to the 4th BPF harmonic. At higher harmonics, a different directivity pattern is observed where patterns and levels, while experimental and analytical ones agree better at higher harmonics.

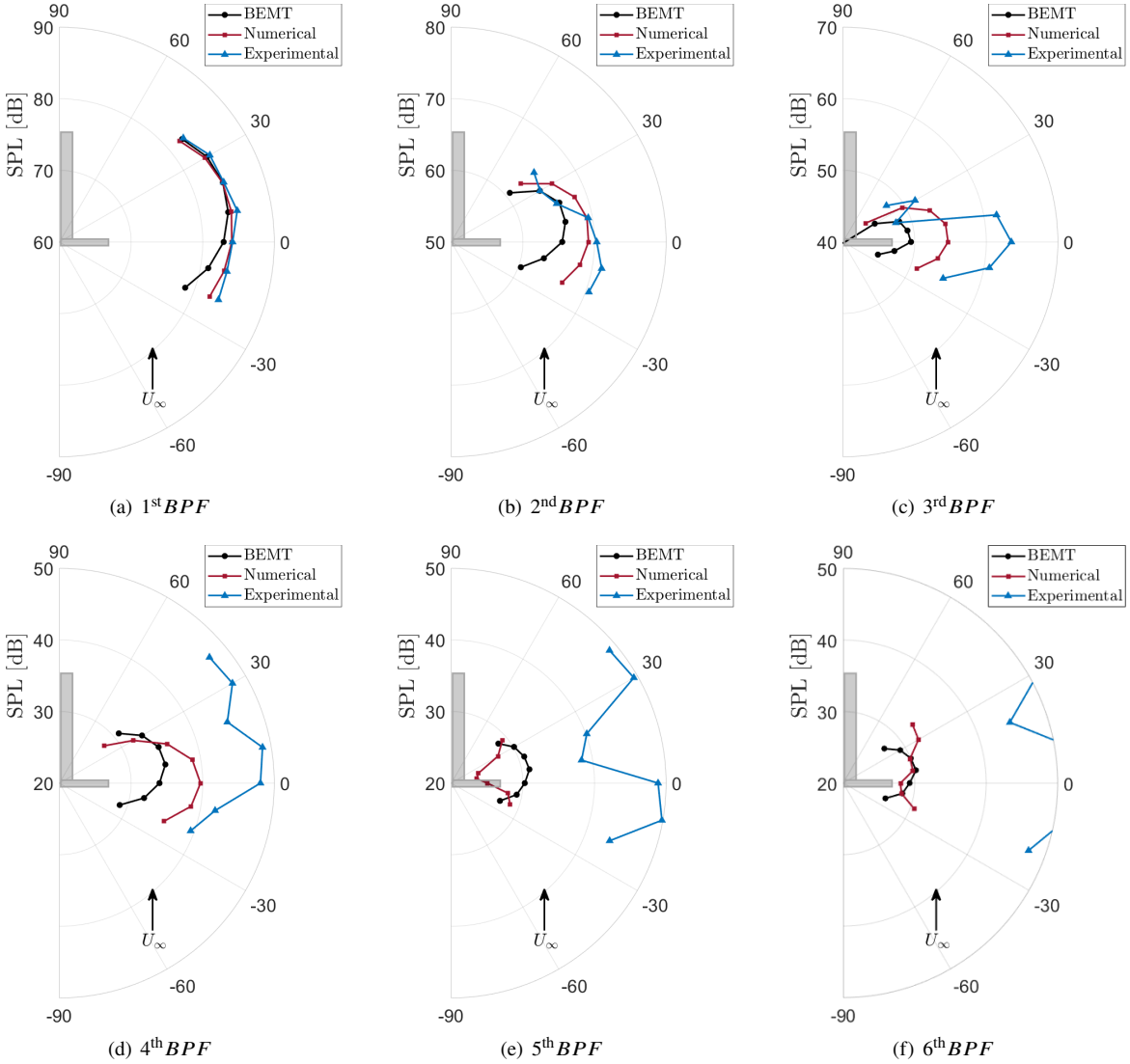

Fig. 7 Experimental, numerical, and BEMT-based average directivity of the noise emmited by the propeller at different harmonics of the blade passing frequency (BPFs).

Figure 8 summarizes the total tonal levels and the discrepancies with respect to the BEMT data. Here the BEMT is taken as a reference due to the experimental uncertainties causing certain BPFs to exhibit significantly different levels. The picture shows clearly the progression of the discrepancies from the first two/three BPF harmonics to the others. In the first harmonic, errors are in ±1.7 dB range (below experimental uncertainties) for the first harmonic. The second and third harmonics see an increase in the errors demonstrated by the underprediction of the analytical methodology and the influence of the motor noise. Higher harmonics yield larger discrepancies, which are significantly lower for the numerical technique in comparison with the experimental one. Here, it must be mentioned that the levels inferred from the experimental campaign reflect levels directly observed in the acoustic spectrum in Figure 5. The former can indicate that the levels obtained from the phase average are still contaminated by broadband noise or that higher tonal components exist in the experiment. The latter can possibly be caused by asymmetries, unsteady loading components,

Downloaded by Technische Universiteit Delft on July 17, 2024 | http://arc.aiaa.org | DOI: 10.2514/6.2024-3267

or other sources of motor noise.

Errors with respect to the numerical technique are dependent on the azimuthal location, and are differences are significantly higher at $\phi = 40^o$ for harmonic numbers above 6. These deviations have two possible sources. First, the load distribution predicted from the BEMT comes from simplifications, with required assumptions on the tridimensionality of the flow and the influence of viscous effects on the blade pressure distribution. These assumptions can lead to differences between the load distribution from the simulations and from the analytical methodology, hence contributing to different noise levels. A second possible source of error is the consideration of compact dipoles from the BEMT-based noise estimations. The latter should affect the high harmonics of the blade passing frequencies, where the blade airfoil geometry and load distribution along the chord can interfere with the noise emission pattern. It must be highlighted that the discrepancies illustrated in this figure correspond to a maximum frequency of around 2670 Hz, equivalent to an acoustic wavelength of around 0.127 m (around 12 times the blade tip chord). This evidence points to the suitability of the compact dipole assumption on the estimation of the demonstrated tonal components. Further investigation, however, requires a full assessment of the load distribution predicted from both methodologies and comparison with experimental results.

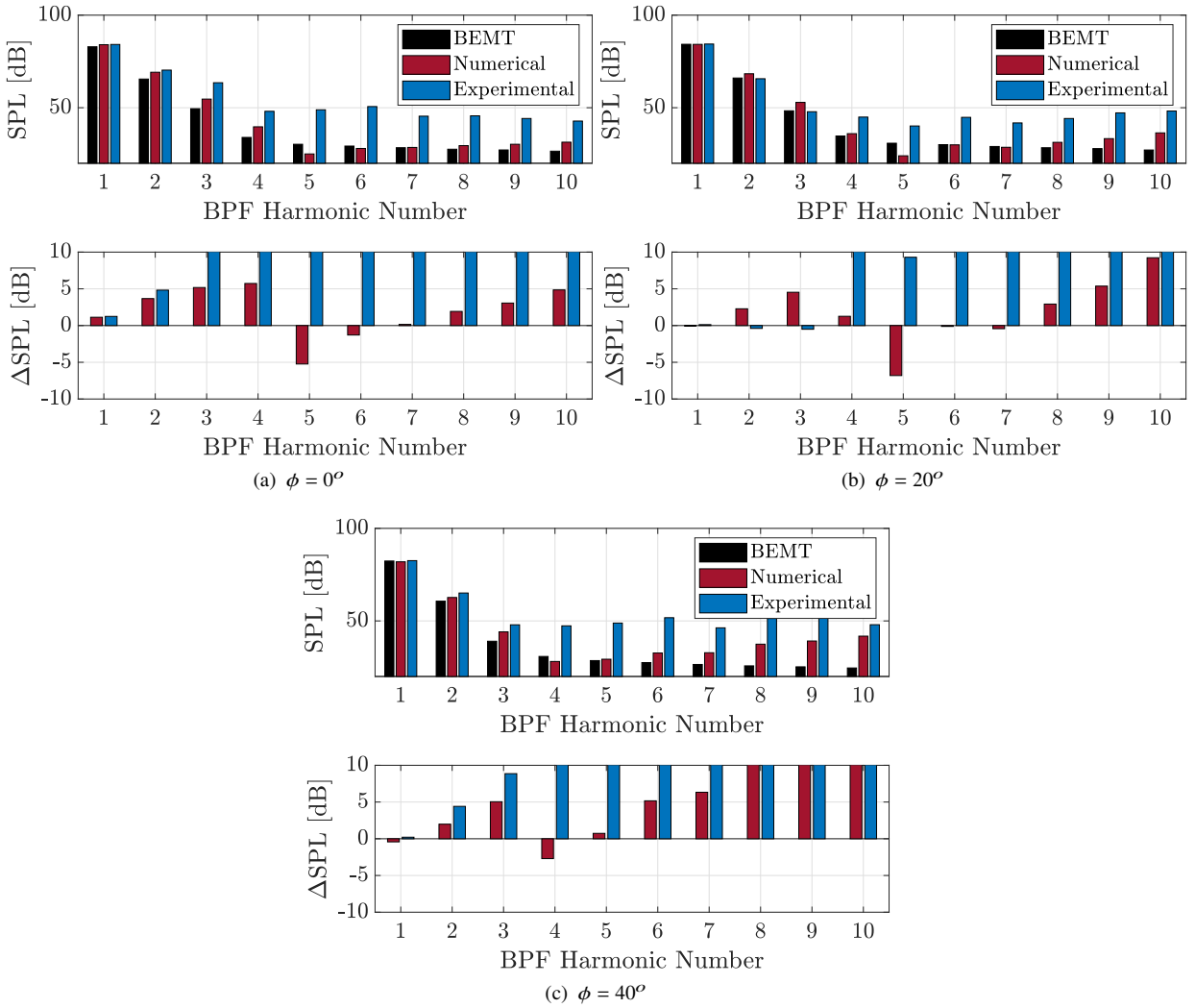

Fig. 8 Comparison of experimental, numerical, and BEMT-based average tonal components at different harmonics of the blade passing frequency (BPF) of the propeller. Relative difference with respect to the BEMT-based estimation is also shown.

Downloaded by Technische Universiteit Delft on July 17, 2024 | http://arc.aiaa.org | DOI: 10.2514/6.2024-3267

VII. Comparisons of broadband noise

The level, spectrum, and directivity of the broadband noise component from the propeller are also compared as this component can dominate the emissions from a propeller operating at low-Reynolds numbers. To remove the tonal component from the broadband signal, a Vold Kalman filter is applied [20]. A second-order filter is applied over a bandwidth of 20 Hz to avoid dampening of the broadband modulation effects. Figure 9 illustrates the effect of the filter on the three signals for an azimuthal angle of $\phi = 0^o$. The figure shows better the broadband amplitude modulation described in Baars et al. [19]. In this image, the modulation is observed both for the experimental and numerical data, with the former demonstrating lower peak levels and higher average levels of broadband fluctuations. This can have particular effects on the perception of noise and a detailed description of the time-history and realist recreation of propeller broadband noise could require considerations on modulation effects.

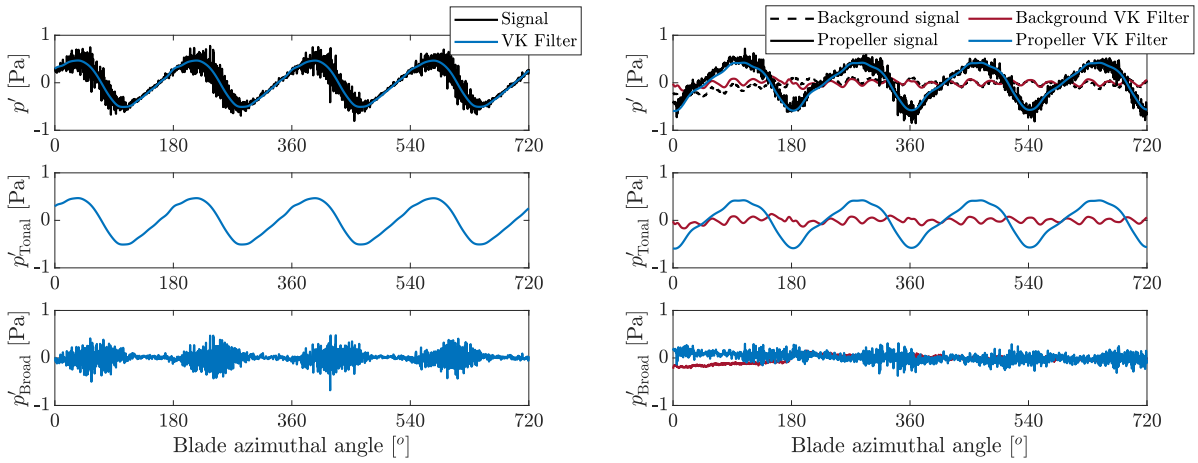

(a) Numerical (b) Experimental

Fig. 9 Example of filtered signal using the Vold-Kalman filtering technique. Time series are taken at azimuthal angle $\phi = 0^o$. (a) shows the results from filtering the numerical data and (b) the experimental one.

The spectra of the broadband fluctuations are shown in Figure 10, where levels are displayed in power spectral density to allow direct comparison of broadband noise. At low frequencies discrepancies are significantly large between BEMT-based, numerical, and experimental predictions. Given background and other possible sources in the experimental data, the levels for frequencies below 1 kHz display no agreement between acoustic emissions from analytical and numerical methods and experimental data. Above 3 kHz numerical, analytical, and experimental predictions are well in agreement. The agreement is best for the lowest azimuthal angle ($\phi = 0^o$). At higher azimuthal angles, experiments demonstrate lower levels in comparison to analytical while numerical ones demonstrate higher levels. The numerical simulations show increasingly higher energies for frequencies above 10 kHz, indicating no decay of the turbulent fluctuations in contrast with analytical estimations and the experimental measurements.

Downloaded by Technische Universiteit Delft on July 17, 2024 | http://arc.aiaa.org | DOI: 10.2514/6.2024-3267

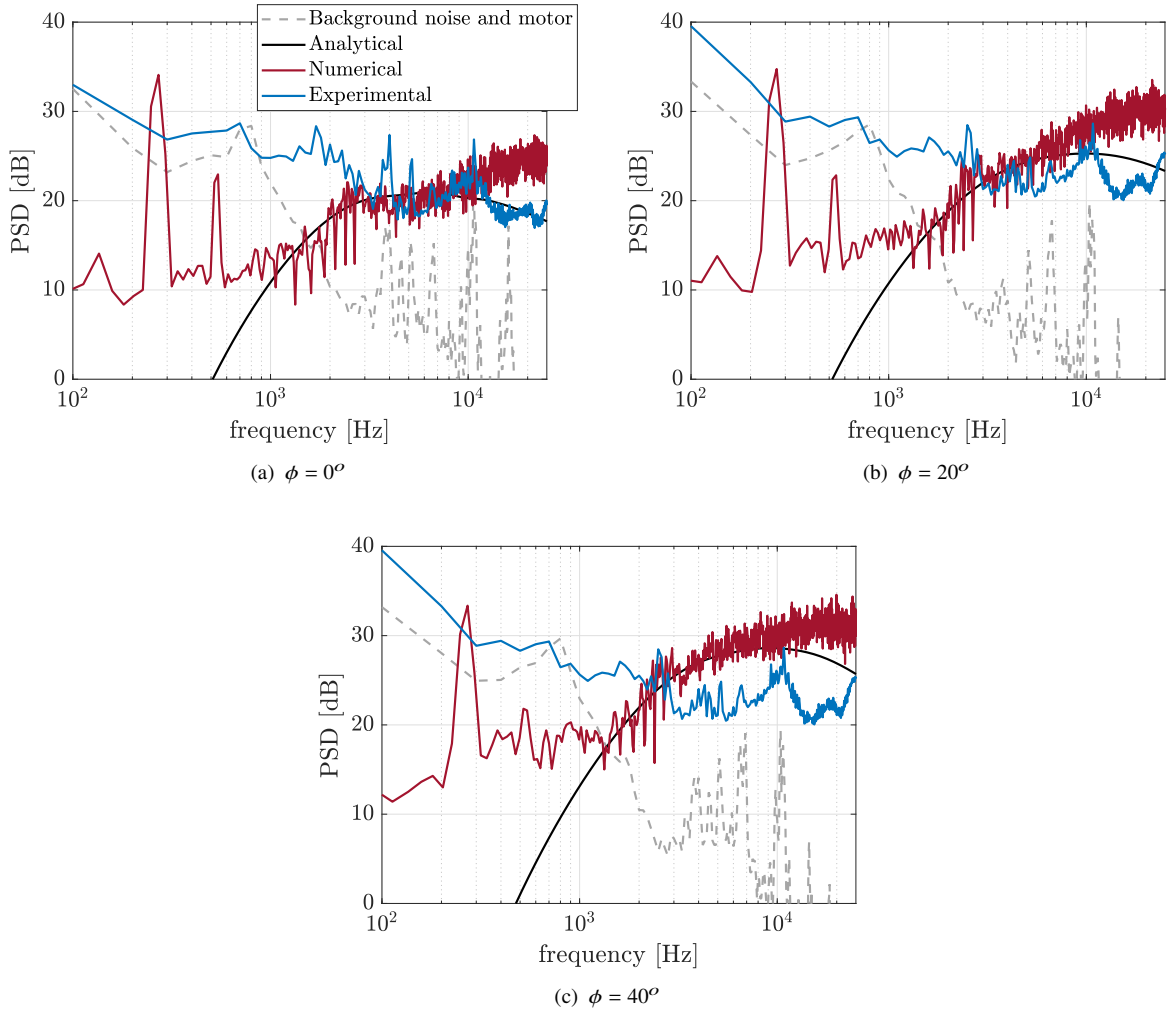

Fig. 10 Experimental, numerical, and BEMT-based Vold-Kalman filtered broadband power spectral density spectrum at different azimuthal angles.

The directivity of the broadband noise emissions is evaluated in Figure 11, where the emissions are evaluated over octave bands derived from the Vold-Kalman filtered data. A dipolar emission pattern, characterized by the lowest levels around the propeller plane is observed for most frequencies, indicating source compactness for the frequencies analysed. At frequencies lower than 2,000 kHz, experiments are dominated by background sources and are far above the predicted levels. Above this frequency, a better agreement between the three methodologies is seen. The agreement confirms the hypothesized dominance of turbulent-boundary layer trailing-edge noise. Discrepancies are well below 5 dB and are the highest for the azimuthal angle $\phi = 40^o$. At the highest frequency, the numerical simulation overestimates the noise emissions in comparison to both other methods. The discrepancies, however, are much slimmer when compared to the tonal components and point to a much more consistent prediction of broadband sources of noise.

Downloaded by Technische Universiteit Delft on July 17, 2024 | http://arc.aiaa.org | DOI: 10.2514/6.2024-3267

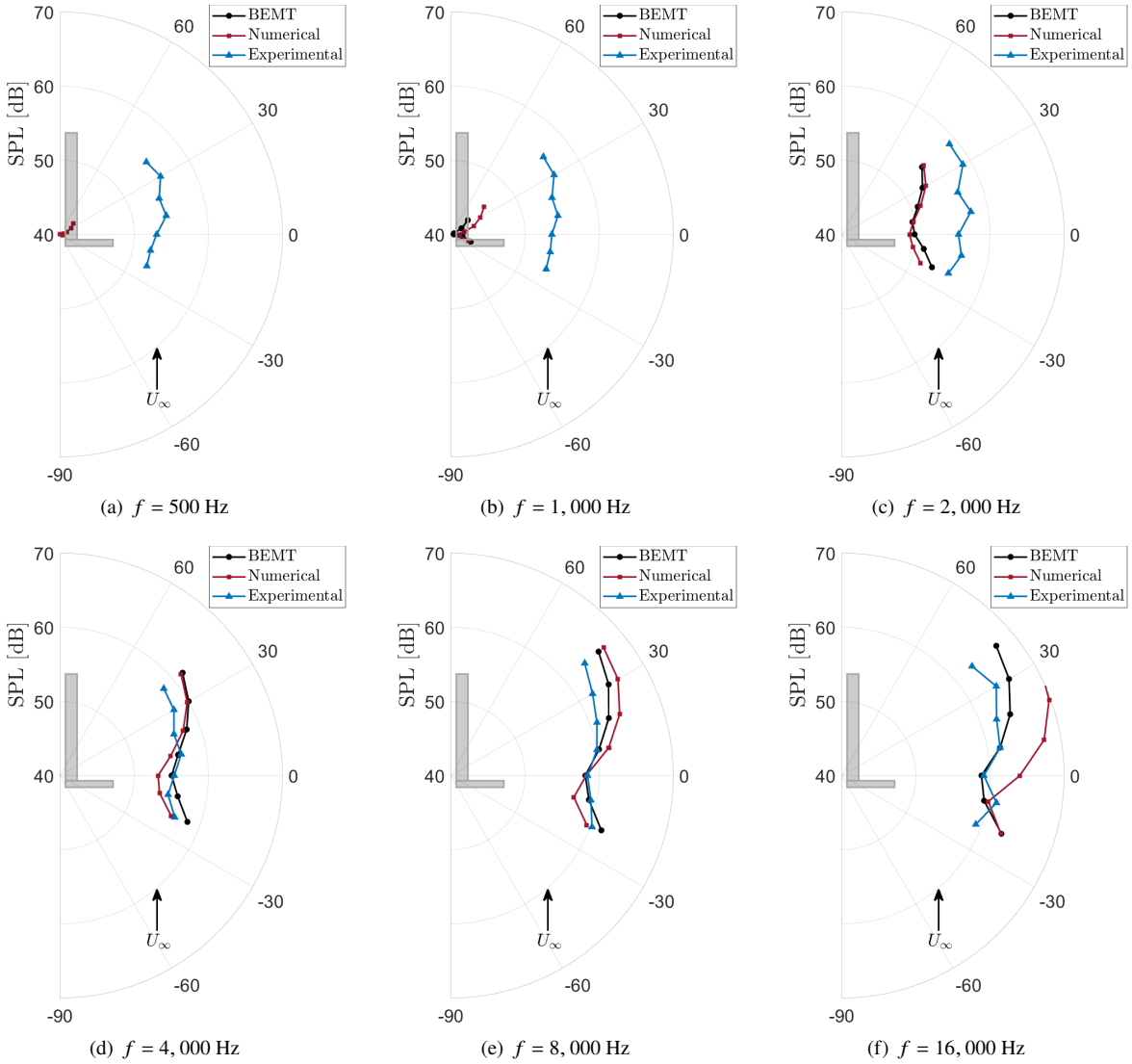

(a) $f = 500$ Hz (b) $f = 1,000$ Hz (c) $f = 2,000$ Hz

(d) $f = 4,000$ Hz (e) $f = 8,000$ Hz (f) $f = 16,000$ Hz

Fig. 11 Experimental, numerical, and BEMT-based average directivity of the broadband noise emmited by the propeller at octave bands.

VIII. Conclusions

This work is dedicated to a comparison of acoustic noise components from isolated propellers. A dedicated experimental campaign is carried out and an equivalent numerical simulation and analytical prediction are conducted. Focus is given to the currently achievable accuracy of high harmonics of the blade passing frequency and broadband sources. A discussion is proposed on the experimental uncertainties incurred from measurements of tonal propeller noise and the accuracy of numerical techniques, sources of discrepancies, and possible mitigation techniques. Comparisons are shown including a BEMT-based noise estimation to propose a discussion on the level of accuracy of the tonal sound pressure levels and its time history along the blade rotation.

Results demonstrate that the three methods are accurate in the description of the first two BPF tonal components, within 3 dB precision and comparable to experimental limitations. These components commonly dominate the acoustic pressure fluctuations from propellers. As a result, the equivalent time history of pressure is well described by the three methodologies. Discrepancies, however, grow as the higher harmonics are to be considered. The latter demonstrates differences between analytical and experimental methods larger than 5 dBs for all harmonics higher than the 3rd blade passing frequency of the blade. Numerical methods demonstrate better agreement with analytical predictions and

Downloaded by Technische Universiteit Delft on July 17, 2024 | http://arc.aiaa.org | DOI: 10.2514/6.2024-3267

discrepancies are only above 5 dBs for harmonic numbers higher than 5. For the latter, errors are particularly higher for large azimuthal angles, where the directionality of the source is predicted inversely to the one suggested by the analytical methodology. Noise from the motors and test rigs is pointed out as one of the causes of the observed discrepancies from experimental measurements. Measurements of the rig without the propellers are shown, collaborating with the hypothesis for 3^{rd}, 6^{th} and 7^{th} harmonic of the blade passing frequency. A final assessment of the sources of discrepancies is not possible due to the different torque requirements and lack of information on possible other sources, i.e. propeller and flow asymmetries.

Broadband signals are separated from the tonal ones with the use of Vold Kalman filtering. Analytical, numerical and experimental methods agree well in the highest frequency ranges (above 2.0 kHz). At such frequencies, all three methodologies display coherent levels and directivities. Discrepancies, in this case, are higher for the numerical methods, which indicate higher levels at high frequencies in comparison to the observed ones from the experiments and the ones predicted analytical. Deviations from the methodologies are in the order of 5 dB at higher frequencies and, mostly, follow the difficulties in predicting the turbulent flow conditions over the blade.

In conclusion, this work stresses the current comparison status of three established methodologies for assessing noise emissions from isolated propellers. The results shown demonstrate that overall noise levels are well-captured, in dB-level precision, for the three methodologies. Nevertheless, a detailed spectral-based description of the emissions requires careful analysis of the results and management of uncertainties and sources of deviation. It is seen that discrepancies grow larger for the higher harmonics of the blade passing frequencies and can be well above 10 dB (one energy scale) between different methodologies. Besides, errors are shown in levels and directivity patterns, which point to different dominant physics between each technique. Similar figures are observed for broadband emissions, where dipolar directivity patterns are observed for all methodologies, indicating discrepancies in the turbulent levels over the blade. The discrepancies are of keen importance in conditions of low-Reynolds numbers and RPM propellers, where increased relative levels of turbulence-based sources and lower human perception of low frequencies cause the higher harmonics of the blade passing frequency and the broadband sources of noise to dominate noise emissions. Following the latter, this work points to the fundamental importance of a more precise description of modelling conditions for numerical simulations, physical description of propeller sources, and, especially, experimental techniques to suppress background and equipment noise sources and assess possible non-symmetric geometric and flow conditions at a deeper level of detail.

Downloaded by Technische Universiteit Delft on July 17, 2024 | http://arc.aiaa.org | DOI: 10.2514/6.2024-3267

References

[1] NASA, "Urban Air Mobility (UAM) Market Study," Tech. rep., 2018.

[2] Rizzi, S. A., Huff, D. L., Boyd, D. D., Bent, P., Henderson, B. S., Pascioni, K. A., Sargent, C., Josephson, D. L., Marsan, M., He, H., and Snider, R., "Urban Air Mobility Noise: Current Practice, Gaps, and Recommendations," *Nasa/Tp-2020*, , No. October, 2020, p. 59. URL `http://www.sti.nasa.gov`.

[3] Kim, J. H., "Urban Air Mobility Noise: Further Considerations on Indoor Space," *International Journal of Environmental Research and Public Health*, Vol. 19, No. 18, 2022. https://doi.org/10.3390/ijerph191811298.

[4] Casalino, D., Romani, G., Zhang, R., and Chen, H., "Lattice-Boltzmann calculations of rotor aeroacoustics in transitional boundary layer regime," *Aerospace Science and Technology*, Vol. 130, 2022, p. 107953. https://doi.org/10.1016/j.ast.2022.107953, URL https://doi.org/10.1016/j.ast.2022.107953.

[5] Casalino, D., Romani, G., Pii, L. M., and Colombo, R., "Flow confinement effects on sUAS rotor noise," *Aerospace Science and Technology*, Vol. 143, No. November, 2023, p. 108756. https://doi.org/10.1016/j.ast.2023.108756, URL https://doi.org/10.1016/j.ast.2023.108756.

[6] Hubbard, H. H., *Aeroacoustics of flight vehicles: theory and practice*, Vol. 1, National Aeronautics and Space Administration, Office of Management . . . , 1991.

[7] Casalino, D., Grande, E., Romani, G., Ragni, D., and Avallone, F., "Definition of a benchmark for low Reynolds number propeller aeroacoustics," *Aerospace Science and Technology*, Vol. 113, 2021, p. 106707. https://doi.org/10.1016/j.ast.2021.106707, URL https://doi.org/10.1016/j.ast.2021.106707.

[8] Romani, G., Grande, E., Avallone, F., Ragni, D., and Casalino, D., "Performance and noise prediction of low-Reynolds number propellers using the Lattice-Boltzmann method," *Aerospace Science and Technology*, Vol. 125, 2022, p. 107086.

[9] Merino-Martínez, R., Rubio Carpio, A., Lima Pereira, L. T., van Herk, S., Avallone, F., Ragni, D., and Kotsonis, M., "Aeroacoustic design and characterization of the 3D-printed, open-jet, anechoic wind tunnel of Delft University of Technology," *Applied Acoustics*, Vol. 170, 2020. https://doi.org/10.1016/j.apacoust.2020.107504.

[10] Grande, E., Ragni, D., Avallone, F., and Casalino, D., "Laminar Separation Bubble Noise on a Propeller Operating at Low Reynolds Numbers," *AIAA Journal*, Vol. 60, No. 9, 2022, pp. 5324–5335. https://doi.org/10.2514/1.J061691.

[11] Farassat, F., and Succi, G. P., "The prediction of helicopter rotor discrete frequency noise," *In: American Helicopter Society*, 1982, pp. 497–507.

[12] Casalino, D., "An advanced time approach for acoustic analogy predictions," *Journal of Sound and Vibration*, Vol. 261, No. 4, 2003, pp. 583–612.

[13] Casalino, D., Barbarino, M., and Visingardi, A., "Simulation of helicopter community noise in complex urban geometry," *AIAA Journal*, Vol. 49, No. 8, 2011, pp. 1614–1624. https://doi.org/10.2514/1.J050774.

[14] Drela, M., and Giles, M. B., "Viscous-inviscid analysis of transonic and low Reynolds number airfoils," *AIAA journal*, Vol. 25, No. 10, 1987, pp. 1347–1355.

[15] Roger, M., and Moreau, S., "Back-scattering correction and further extensions of Amiet's trailing-edge noise model. Part 1: Theory," *Journal of Sound and Vibration*, Vol. 286, No. 3, 2005, pp. 477–506. https://doi.org/10.1016/j.jsv.2004.10.054.

[16] Schlinker, R. H., and Amiet, R. K., "Helicopter Rotor Trailing Edge Noise," *NASA Contractor Report 3470*, 1981, p. NASA.

[17] Goyal, J., Sinnige, T., Ferreira, C. S., and Avallone, F., "Aerodynamics and Far-field Noise Emissions of a Propeller in Positive and Negative Thrust Regimes at Non-zero Angles of Attack," , No. June, 2023, pp. 1–27. https://doi.org/10.2514/6.2023-3217.

[18] Monteiro, F. d., Ragni, D., Avallone, F., and Sinnige, T., "Low-order acoustic prediction tool for estimating noise emissions from distributed propeller configurations," 2023. https://doi.org/10.2514/6.2023-4180.

[19] Baars, W. J., Bullard, L., and Mohamed, A., "Quantifying modulation in the acoustic field of a small-scale rotor using bispectral analysis," *AIAA Scitech 2021 Forum*, 2021, p. 0713.

[20] Vold, H., Mains, M., and Blough, J., "Theoretical foundations for high performance order tracking with the Vold-Kalman tracking filter," *SAE transactions*, 1997, pp. 3046–3050.

Downloaded by Technische Universiteit Delft on July 17, 2024 | http://arc.aiaa.org | DOI: 10.2514/6.2024-3267